ELSEVIER

Journal of Structural Geology 28 (2006) 64–82

JOURNAL OF STRUCTURAL GEOLOGY

www.elsevier.com/locate/jsg

Can belemnite distribution reveal pressure-solution processes along faults? A case study in the chalk of the Mons Basin, Belgium

J. Angelier[a,*], S. Vandycke[b], F. Bergerat[c], P. Gaviglio[d], C. Schroeder[e], M. Coulon[f]

[a]*Observatoire Océanologique de Villefranche, UFR 939 Université Pierre-et-Marie Curie & UMR 6256 Géosciences Azur, BP 48, 06235 Villefranche-sur-Mer cedex, and Institut Universitaire de France, France*

[b]*FNRS, Faculté Polytechnique de Mons, Géologie fondamentale et appliquée, 9 rue de Houdain, 7000 Mons, Belgium*

[c]*Laboratoire de Tectonique, Université Pierre et Marie Curie, FR 32 CNRS-UPMC, CEPAGE, case 117, 4 place Jussieu, 75252 Paris, France*

[d]*EA 2642 Géosciences, Université de Franche-Comté, 16 Route de Gray, 25030 Besançon cedex, France*

[e]*GEOMAC, Université de Liège, Chemin des Chevreuils, 1, B52/3, 4000 Liège; ULB, Lab. Jacques Verdeyen, av. Roosevelt, 1050 Brussels; UCL, Dept Génie Civil & Environnement, 1459 Louvain-La-Neuve, Belgium*

[f]*Laboratoire des Sciences de la Terre, CRA, 2, esplanade Roland Garros, 51100 Reims, France*

Received 8 November 2004; received in revised form 4 August 2005; accepted 8 August 2005
Available online 10 October 2005

Abstract

A detailed study of normal faults in the calcarenites and chalks of the Mons Basin reveals that pressure-solution processes play a significant role in fault zones, which affects the determination of the amounts of extension. Drag folding associated with normal simple shear and rock dissolution concurred to produce layer flexuring in the hanging wall of the normal faults, whereas the footwall remained almost intact. Analysing the distribution of fossil belemnite rostra in and away from fault zones enabled us to evaluate these effects. The sense and amount of belemnite tilt constrain the minimum thickness of dissolved hanging wall fringe, revealing significant pressure-solution in addition to drag folding. We developed 2-D and 3-D analytical models of along-fault belemnite rotations induced by drag folding and dissolution, and we applied these models to our data from the Mons Basin. The results show that the pressure-solution effect is significant, implying a smaller ratio between horizontal and vertical components of motion than expected. It follows that the across-fault amount of extension is smaller than that predicted from the single fault geometry, suggesting that although the existence of Campanian–Maastrichtian–Danian extension in the Mons Basin area is beyond doubt, its amplitude should not be overestimated.

Keywords: Normal faults; Drag folding; Simple shear; Pressure-solution; Dissolution; Belemnite; Chalk; Calcarenite; Cretaceous; Mons Basin

1. Introduction

Numerous studies have highlighted close interaction between faulting and pressure-solution processes (Ramsay, 1977; Hancock, 1985; Gratier, 1987; Carrio-Schaffhauser and Gaviglio, 1990; Dunne and Hancock, 1994; Peacock et al., 1998). In chalk, the dissolution and migration of calcium carbonate and its relation to stress was discussed by Mimran (1977), based on examples from the Isle of Wight and Dorset. However, relatively little is known concerning the quantification of dissolved material along faults and fractures. Whether or not pressure-solution phenomena are closely related to, and quantitatively influence, the development of tectonic basins is generally poorly documented.

In western Belgium, the Mons Basin area experienced simultaneous chalk sediment deposition and normal faulting during the latest Cretaceous (late Campanian–lower Maastrichtian). Not only did tectonic analyses in the chalk layers reveal widespread normal faulting (although most offsets remained small), but they also provided evidence of syndepositional tectonism (Vandycke et al., 1991).

Typical pressure-solution features, such as stylolitic joints, are uncommon in the chalk of the Mons Basin. Few stylolitic peaks could be found but were very small. This poor development of stylolites is a consequence of specific chalk properties, especially high porosity.

* Corresponding author. Tel.: +33 4 93 76 37 54; fax: +33 4 93 76 37 66.
E-mail address: jacques.angelier@geoazur.obs-vlfr.fr (J. Angelier).

0191-8141/$ - see front matter © 2005 Elsevier Ltd. All rights reserved.
doi:10.1016/j.jsg.2005.08.007

Pressure-solution remains diffuse in chalk, in contrast with compact limestones where water circulation commonly occurs along joints.

Qualitative data, however, revealed syntectonic pressure-solution phenomena in the white chalk formation, Campanian in age. Some partly dissolved belemnites were found in faults (Marlière, 1970). Later, petrophysical analyses revealed that solution phenomena affect narrow zones, a few centimetres wide, along faults. It could thus be suggested that 'the extensional deformation of the Mons Basin might have been partially hindered by chemically induced matrix strains' (Gaviglio et al., 1999). These analyses further provided some evaluation of the minimum pressure-solution shortening based on the reduction of porosity observed in a fault-perpendicular thickness from 0.09 to 0.18 m (see Table 3 in Gaviglio et al., 1999). Dissolution probably occurred across some sets of joints but pressure-solution seams do not show structures that would allow quantification of dissolution processes.

In this paper we aim to better characterise the balance between the pressure-solution phenomena and the slip-related deformation along faults, based on consideration of specific benchmarks: the belemnite fossils. It has been observed that close to faults belemnites often show steep tilt angles that are uncommon at larger distances from faults (Gaviglio et al., 1999). We consequently carried out systematic measurements of belemnites in the two chalk formations of the Mons Basin, and we paid particular attention to their relation to faults, in terms of both the orientations and the distances.

Based on quantitative analysis of the rotations that affected belemnites near faults, the main questions addressed hereafter, deal first with the importance of pressure-solution processes along faults as compared with drag folding that also occurs, and second with the correction of biases in estimates of extension rates as a function of normal faulting. The answers to these questions are expected to highlight the role of pressure-solution phenomena in the development of the basin, especially during deposition, compaction and diagenesis.

The principle of our study is simple: because belemnite fossils composed of dense crystalline calcite were much less affected by pressure-solution phenomena than the host chalk sediment composed of micron-scale coccolith debris, they can be used as benchmarks to reconstruct and quantify deformation and dissolution processes. In our study, we focus on the Campanian–Maastrichtian sediments, in which belemnite fossils are common.

2. Structure and Late Cretaceous deformation of the Mons Basin

The Mons Basin, a northern extension of the Paris Basin (Fig. 1a), is filled with Cretaceous–Tertiary sediments, mainly chalks, calcarenites, marls, silts and clays. Except along fault-flexure zones where the layers locally dip as steeply as 60°, the bedding dips are shallower than about 10° (Fig. 1b). Chalk and calcarenite dominate in the Turonian–Danian section. The cumulative thickness of the Cenomanian–Lutetian sedimentary sequence, 800 m, is never reached in real section (about 200 m thick) because of depocentre migrations during basin evolution. Structural analyses revealed close relationship between depocentres and normal faults active during the Late Cretaceous and Early Tertiary (Vandycke et al., 1991). Most observations and measurements used in this paper were collected in the Campanian–Maastrichtian chalk–calcarenite formations (Fig. 1c).

A detailed tectonic investigation has been carried out in the chalky formations in order to reconstruct paleostress regimes and the evolution of tectonic stress. The Late Cretaceous history of faulting was revealed by sealed normal faults, changes in sediment thickness across normal faults, and relative chronology between brittle structures. The most frequent brittle structures are dip-slip normal faults and tension fractures revealing a succession of syndepositional and post-depositional normal faulting events. Joints are common in the Campanian white chalk and rare in the overlying calcarenites.

The Maastrichtian was a period of tectonic activity in this region of Europe (Vandycke, 2002). Strike-slip faulting occurred during the early Maastrichtian, when the E–W North Artois Shear Zone (Colbeaux, 1974) was active beneath the Mons Basin as a crustal zone of dextral strike-slip (Vandycke et al., 1988; Vandycke and Bergerat, 1989), but played a minor role in terms of basin evolution. Normal faulting was closely related to the sedimentary history of the Mons Basin, with NW–SE-trending extension during the upper Campanian, followed by NE–SW-trending extension during the Maastrichtian. The NE–SW extension was continuing during the early Eocene. The later tectonic evolution was mainly characterised by NE–SW extension interrupted by structural inversion events (especially during the Late Eocene–Oligocene), and the present-day stress regime involves NE–SW extension and NW–SE compression. These post-Maastrichtian events have little relevance for our study, in which emphasis is put on pressure-solution processes related to earlier tectonic episodes.

Whether Late Cretaceous faulting in the Mons Basin resulted from extension or from vertical movements was a matter of debate. Block subsidence was attributed to dissolution of Carboniferous anhydrite in the Paleozoic basement by Delmer (1972). Dupuis and Vandycke (1989) drew attention to the importance of karstic subsidence during the Early Cretaceous period; they also pointed out that extensional tectonic activity during and after the Cretaceous played a role in the development of the Mons Basin (Vandycke et al., 1991).

Determining the actual amounts of extension across normal faults is crucial, because the horizontal deformation

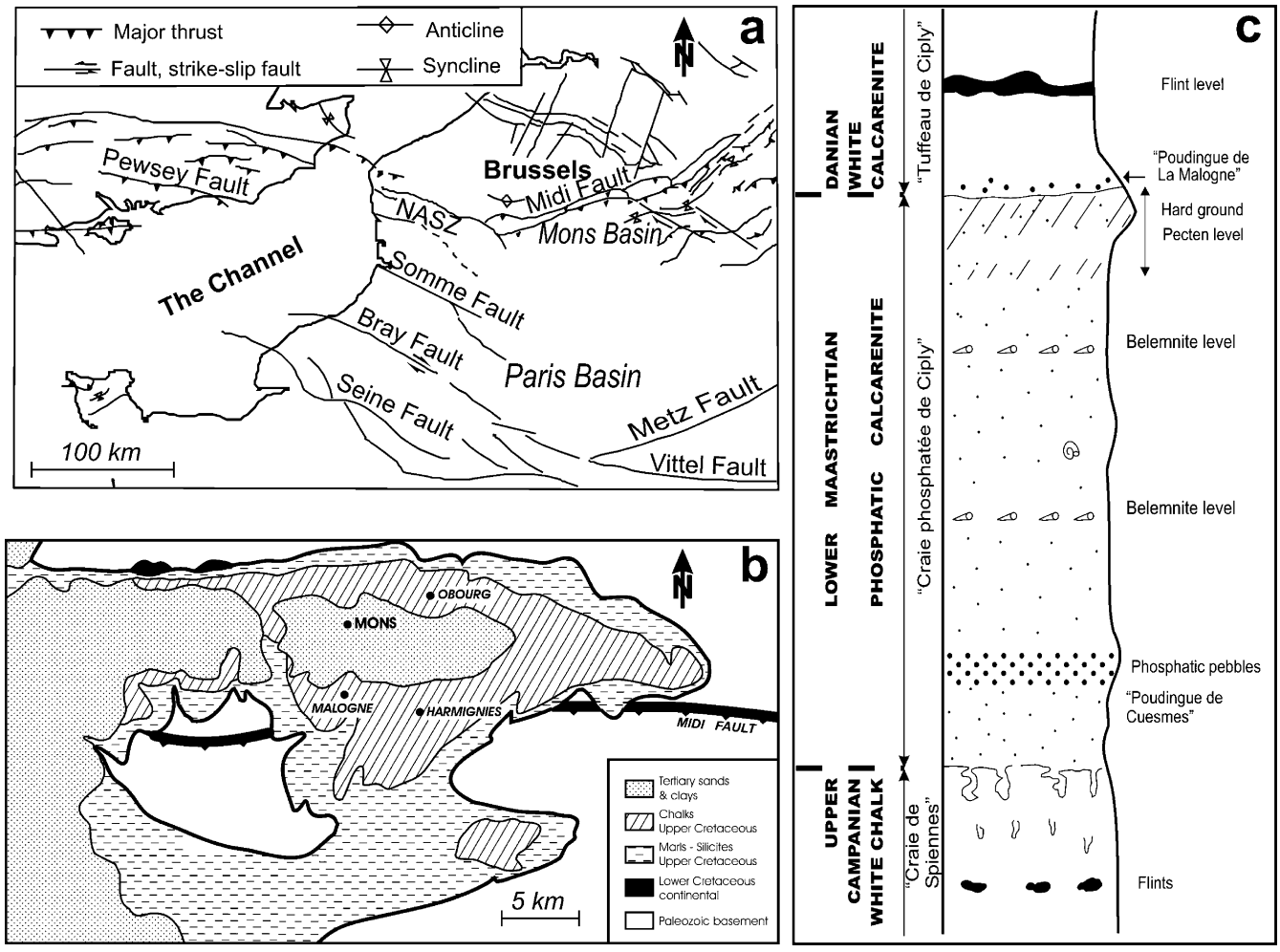

Fig. 1. Location and geological setting of studied area. (a) Geological map of northern Paris Basin. Rectangular frame: location of Mons Basin. (b) Geological map of Mons Basin, with location of the main studied sites (Harmignies, Obourg and La Malogne chalk quarries). (c) Stratigraphic succession, late Campanian–lower Maastrichtian formations of Mons Basin.

perpendicular to normal fault trend combines extension resulting from shear and shortening resulting from pressure-solution processes. If these two terms are equal, the brittle tectonics of the Mons Basin could be merely explained by vertical movements (e.g. a consequence of dissolution in the basement). Such a possibility would poorly account for the high levels of structural organisation observed in the normal fault patterns of the Mons Basin (Vandycke, 1992). These patterns reveal characteristic trends suggesting far-field extension, rather than the irregular trends that would be generated by local, gravity-induced vertical movements. However, the steep fault dips (in the range 60–90°, with a peak at 70–80°) suggest that the amplitude of horizontal extension is small with respect to vertical block displacement.

3. Shear versus pressure-solution: the problem

Previous analyses in the chalk formations of the Mons Basin showed that dissolution–crystallisation phenomena, related to water circulation along faults and coeval with normal faulting, played a significant role (Gaviglio et al., 1993, 1999), and therefore must be taken into account while determining effective amounts of extension. The properties of chalk formations deserve specific attention (e.g. Clayton and Matthews, 1987). Petrophysical studies based on analyses of porosity, elastic wave velocity, capillary rise and permeability revealed noticeable matrix strains mainly due to pressure-solution along fault surfaces. The transformations involve significant reduction in volume, change in access diameter of porous network and higher rock heterogeneity over a 0.10–0.15-m-wide zone along the fault.

How these changes may influence the fault-related deformation is highlighted by considering two end members: extensional faulting without dissolution (Fig. 2a) and dissolution in fault zone without extension (Fig. 2b). In the first case, the motion vector is parallel to the fault. In the second case, dissolution affects a fault-parallel zone and the relative motion is vertical. The presence of a

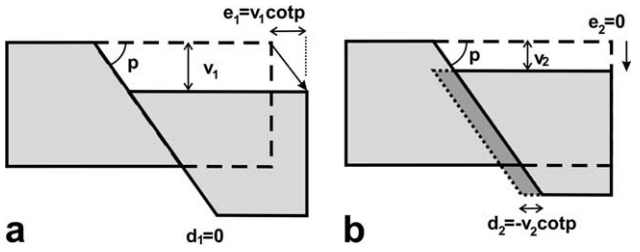

Fig. 2. Theoretical scheme illustrating the relationship between horizontal extension, e, and vertical motion, v, related to normal faulting. The dip of the normal fault is p. (a) Normal faulting without dissolution. (b) Vertical motion accommodated by dissolution.

fault was, however, necessary because it favoured water circulation, and hence dissolution inside the adjacent rock mass. As a consequence, the situation of Fig. 2b, with dissolution alone, represents a theoretical end member that is probably never reached. A pressure-solution-related shortening larger than normal fault-related extension does not deserve consideration because layers of insoluble material offset by normal faults did not show significant near-fault shortening (e.g. flint levels in Danian calcarenites), or revealed shortening smaller than fault-related extension (e.g. phosphatic nodule levels in Maastrichtian chalk), as shown by Vandycke et al. (1990). Fig. 2 thus presents the two end-members of all possible situations across the normal faults of the Mons Basin, which may involve simple shear and dissolution in variable proportions.

In the absence of dissolution, and assuming constant rock volume, the ratio between the horizontal extension across a normal fault, e_1, and the vertical component of motion on the same fault, v_1, is a function of the fault dip, p (Fig. 2a). By definition, the horizontal width of the rock dissolved along the fault, d_1, is zero.

$$e_1 = v_1 \cot p. \tag{1}$$

As the opposite end-member, pure vertical motion, v_2, is entirely accommodated by rock dissolution along a non-vertical plane (Fig. 2b). The horizontal width of the rock dissolved by pressure-solution along the fault, d_2, thus compensates the transverse horizontal offset of the fault. In this case, the effective horizontal displacement, e_2, reduces to zero and the horizontal width of dissolved rock, d_2, is given by expression (2):

$$d_2 = v_2 \cot p. \tag{2}$$

If normal faulting and dissolution occur in variable proportions (the actual case), the resulting vertical motion, v, is the sum $v_1 + v_2$, while the resulting horizontal extension perpendicular to fault trend equals e_1 (because $e_2 = 0$). The quantity $v \cot p$ is easily calculated for each observed fault, and one writes

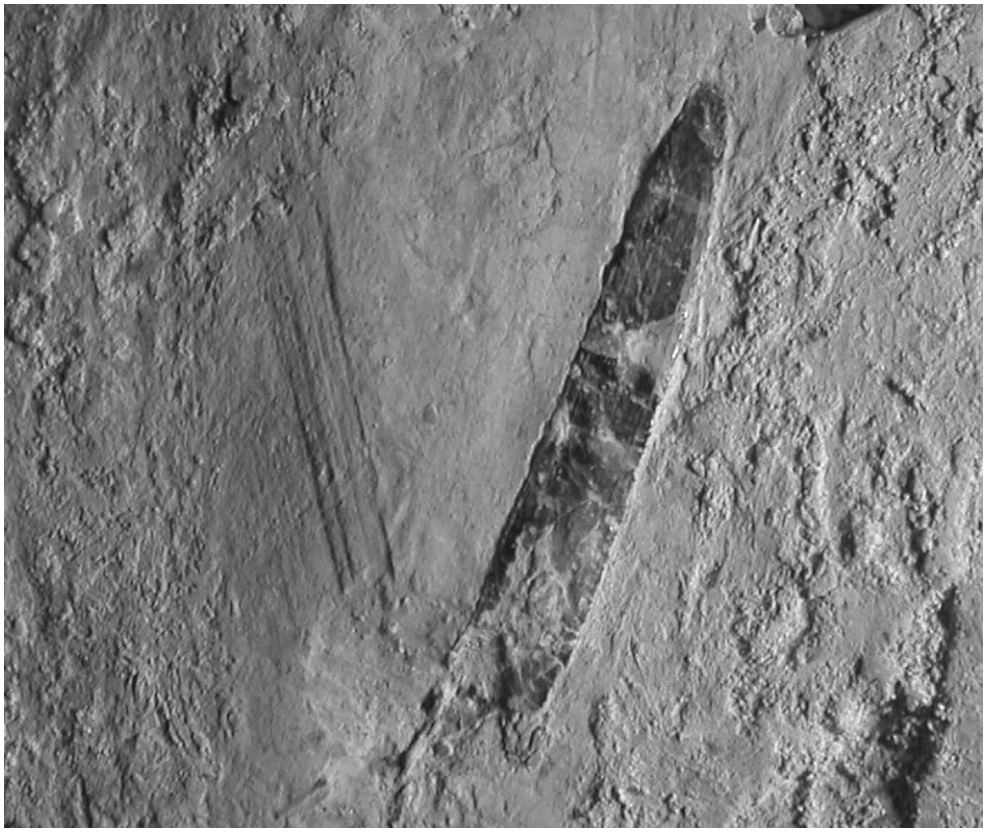

Fig. 3. Belemnite rostrum tilted along normal fault until fault-parallel position, and affected by dissolution so that only one half remains. Note slickenside lineations on fault surface (on left). White chalk, Harmignies quarry, Mons Basin.

$$v \cot p = e_1 + d_2, \quad (3)$$

which indicates that for a given vertical offset and fault dip, v and p, respectively, the sum of the extension related to normal faulting and the horizontal shortening resulting from pressure-solution is constant. Eq. (3) can be used to define bounds for the components e_1 and d_2.

Although most belemnite plunges remain shallow in the nearly horizontal formations of the Mons Basin, steep plunges have been noticed along several normal faults (Fig. 3). This particular distribution may result from drag folding or pressure-solution processes. Because belemnite fossils had a rigid behaviour, their present-day attitudes provide access to along-fault deformation. Some belemnites underwent dissolution along faults (Fig. 3), but at a much lesser degree than the host rock, which provides access to pressure-solution phenomena. We intend to use the spatial distribution of belemnites as a key to investigate the relative importance of these two processes.

4. Pressure-solution versus shear and drag folding

4.1. Behaviour of chalk, calcarenite and belemnites

Reconstructing the near-fault deformation in the white chalk formation is difficult because the rock is homogeneous and the stratigraphic markers (e.g. hard grounds) are few. We carried out additional investigation in the phosphatic calcarenite 'Craie Phosphatée de Ciply', which contains dissolution-resistant stratigraphic markers such as phosphatic gravel beds and ferrugineous levels, and hence allows easier reconstruction of deformation along faults. Several sections showed that drag folds with amplitudes in the range 0.1–1 m exist on the hanging wall side of many normal faults (Fig. 4). In addition, the layers that contain relatively insoluble material often become thicker near faults (Fig. 4c). This concentration of insoluble material indicates that dissolution has occurred near the fault. The thickening associated with the accumulation of insoluble material thus reveals a large horizontal component of dissolution-related deformation. Had this dissolution acted in the vertical direction, the layer would now be thinner near the fault, not thicker.

Both the drag fold effect and the pressure-solution along normal faults may result in tilting of the belemnites. Tilted belemnites with dip-slip attitude along faults are common in the Mons Basin, incompatible with drag folding taken alone. Considering a belemnite rostrum with a nearly horizontal attitude before deformation, reaching plunges of 70–80° would require unrealistic amounts of simple shear (Fig. 5a–c). In contrast, dissolution has full capacity to produce such large rotations (Fig. 5d–f). To take advantage of this difference between shearing and pressure-solution effects, we undertook a campaign of systematic measurement of belemnite orientations close to normal faults.

Belemnites are common fossils in the chalk formations of the Mons Basin. Most of them belong to two species, *Belemnitella mucronata mucronata* (Schloteim) and *Belemnella* cf. *obtusa* Schulz (Robaszynski and Christensen, 1989). The first species is mainly found in the white chalk, late Campanian in age, and the second species is frequent in the 'Craie Phosphatée de Ciply', early Maastrichtian in age. The common rostrum size falls in the range 0.04–0.15 m for *Belemnitella mucronata* and 0.05–0.10 m for *Belemnella* cf. *obtusa*. The rostra are made of compact crystalline calcite and thus more resistant to dissolution than the surrounding porous chalk matrix. Examples of belemnites partly affected by dissolution exist but remain scarce (Fig. 3). Because of their difference with host rock in structure and response to dissolution, the belemnites are good markers for evaluating pressure-solution phenomena. To some extent, this property is highlighted by the higher density of belemnite fossils along fault surfaces, as compared with their frequency in the adjacent chalk layers.

4.2. Effect of along-fault simple shear and pressure-solution on belemnites

In the chalk layers of the Mons Basin, many Belemnites rostra steeply plunge along, or close to, fault surfaces. At larger distances from faults such steep plunges are exceptional. Faulting-related drag folding and pressure-solution are responsible for these abnormal steep plunges. The belemnite rostrum shown in Fig. 3 has been tilted along a dip-slip normal fault, now being parallel to fault surface. Had dissolution been absent, this situation would imply an amount of simple shear much larger than that allowed by the observed offset. Only one half of the belemnite has been preserved, the section being parallel to rostrum axis. Detailed observation of the rostrum section revealed that the fossil had not been longitudinally cut and offset by the fault, but submitted to dissolution. The fault-parallel section of the belemnite shows a glossy aspect without slip-related striae, although slickenside lineations are common on the fault surface (Fig. 3). This observation is not surprising in light of the evidences for pressure-solution along faults brought by the petrophysical analyses mentioned in Section 3. Gaviglio et al. (1999) concluded that the steep plunges of belemnites near fault planes might result from pressure-solution phenomena along faults.

Observation of belemnites in tabular domains at large distances from the faults showed a variety of plunges, so that it cannot be assumed that the belemnites were horizontal prior to faulting and dissolution processes. Belemnites were commonly eaten by marine vertebrates, with their rostra being rejected in sea water (Hauff, 1985). Most of these plunges are nearly horizontal within a $\pm 20°$ range, in agreement with a simple model of cylindrical fossils falling on the flat bottom of the sea. This plunge dispersion cannot be neglected with respect to tectonic

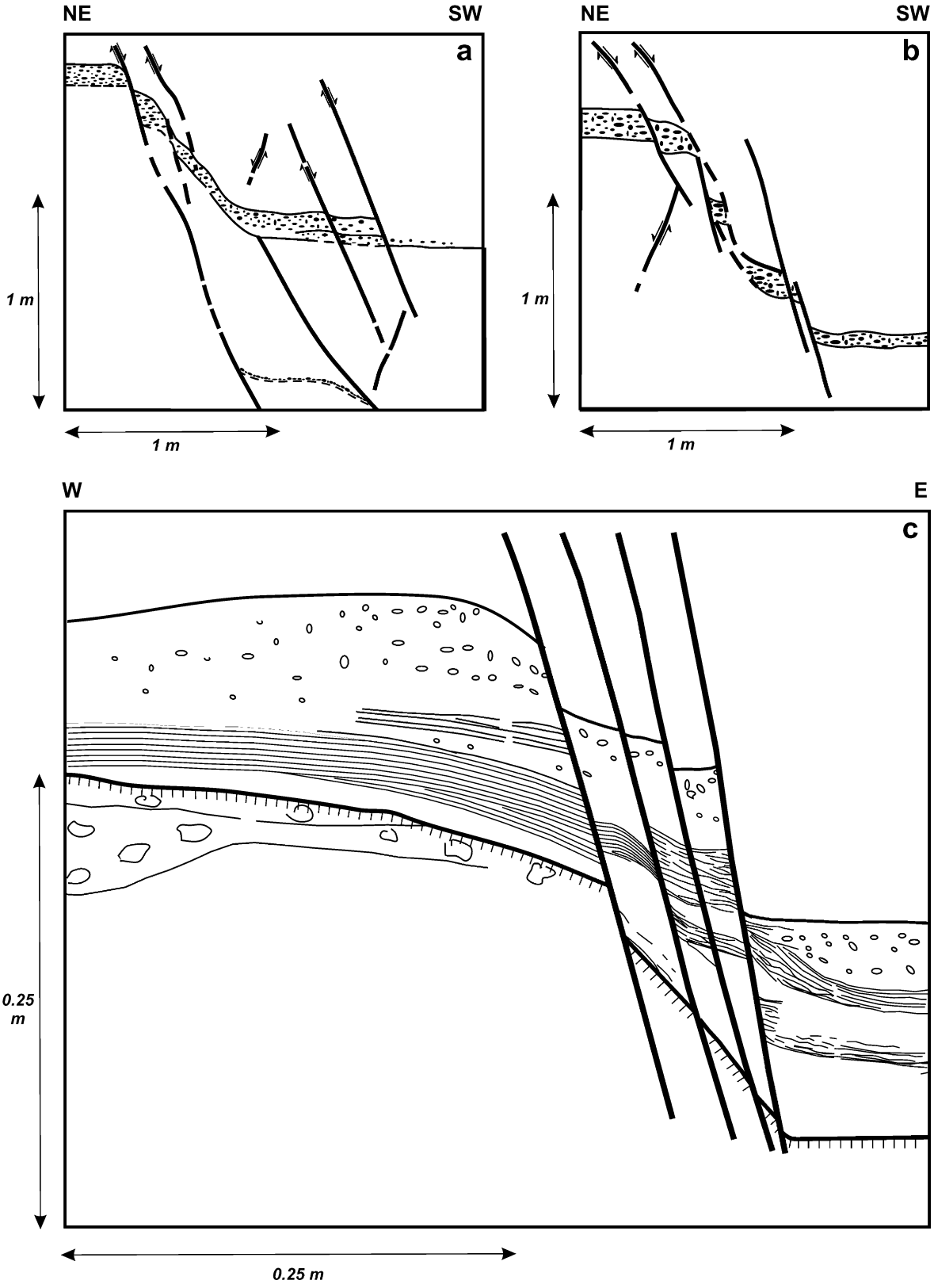

Fig. 4. Examples of cross-sections of minor normal faults showing drag folding associated with dissolution. Calcarenite formation 'Craie Phosphatée de Ciply', La Malogne underground quarry. Homogeneous calcarenite in white or light grey, phosphatic gravels as dotted pattern, levels with ferruginous clay as thin layer-parallel lines, faults as thick lines, hard-ground surface as thick line with barbs. Note variations in thickness in phosphatic gravel layers (all sections) and evidence of syndepositional faulting (bottom-section).

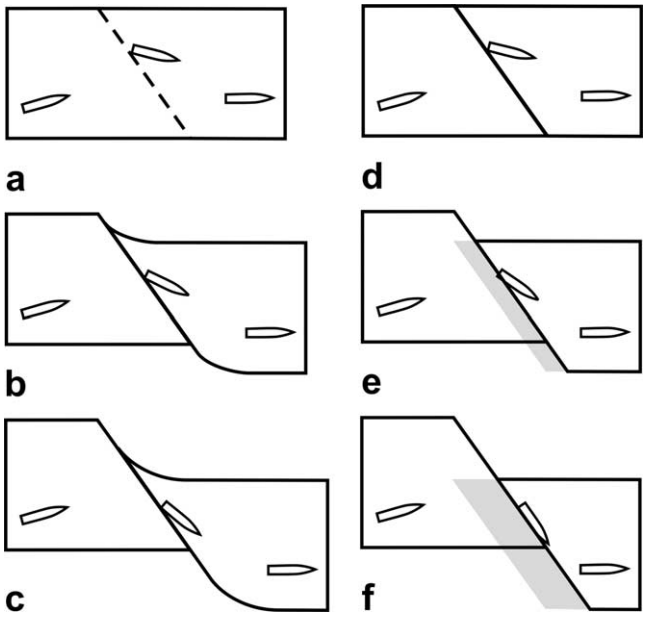

Fig. 5. Theoretical scheme illustrating the tilting of belemnite related to shear along normal fault and drag folding without dissolution (on left) or pressure-solution without shear (on right). Same end-members situations as in Fig. 2. (a) and (d) Initial stage, with horizontal or shallow plunging belemnites in rock mass. (b) and (c) Increasing drag folding in the hanging wall related to ongoing normal faulting and extension, with progressive tilt of near-fault belemnite. (e) and (f) Increasing removal of rock (light grey) in the hanging wall block because of pressure-solution along a pre-existing discontinuity. Note the progressive tilt of the near-fault belemnite in both cases and the dip-slip final attitude in the dissolution case. Note also the contrast between increasing width indicating extension ((a)–(c)) and constant width indicating pure vertical displacement ((d)–(f)).

rotation, precluding a direct interpretation of belemnite plunges in terms of tilting.

Fig. 5 describes the same end members of the actual faulting-dissolution process as in Fig. 2 and shows the corresponding rotations of belemnites. If drag folding occurs alone, the maximum rotation of the belemnite is function of the amount of simple shear but cannot exceed a certain value (Fig. 5a–c). If dissolution occurs alone, massive pressure-solution affects the chalky matrix within a fault-parallel zone and the rotation of the solution-resistant belemnite is a direct consequence of this fault-perpendicular shortening (Fig. 5d–f). To this respect, it is important to keep in mind that in the porous chalk the dissolution is not restricted to the fault surface (which would make rotation difficult). Instead, dissolution invades a certain thickness perpendicular to the fault surface (0.09–0.18 m according to Gaviglio et al. (1999)). To highlight the difference between the situations of Fig. 5, one may consider a horizontal belemnite perpendicular to fault trend that finally reaches a dip-slip attitude along the fault. In the drag folding case, infinite simple shear is required. In the pressure-solution case, removing a rock thickness that equals the belemnite length is enough.

Additional observations indicate that pressure-solution plays a major role near faults. For instance, based on DEM photographs, Gaviglio et al. (1997) described a near-fault packing of chalk grains much denser than in the chalk volumes located away from the rotated belemnites. The pervasive behaviour of dissolution was probably facilitated by the soft nature of the sediments, as most normal faults of the Mons Basin predated complete diagenesis.

As noted earlier in this section (Fig. 5), shear and dissolution processes are not equivalent in terms of rotations of rigid bodies near the fault. These two processes are quantitatively analysed in Fig. 6. In the first case, a belemnite undergoes shear in the drag fold zone along the normal fault (Fig. 6a). This process is controlled by the shear angle, ψ. In the second case, a belemnite is preserved from dissolution and rotates in the pressure-solution zone (Fig. 6b). This process is controlled by the thickness of rock that disappeared because of dissolution, s, knowing that pressure-solution occurs within a zone broader than s. Note that s is measured perpendicular to fault plane, and thus represents $d_2 \sin p$ in Fig. 2b.

Let us consider the case of a belemnite in a vertical plane perpendicular to fault strike. From this simple case analysis

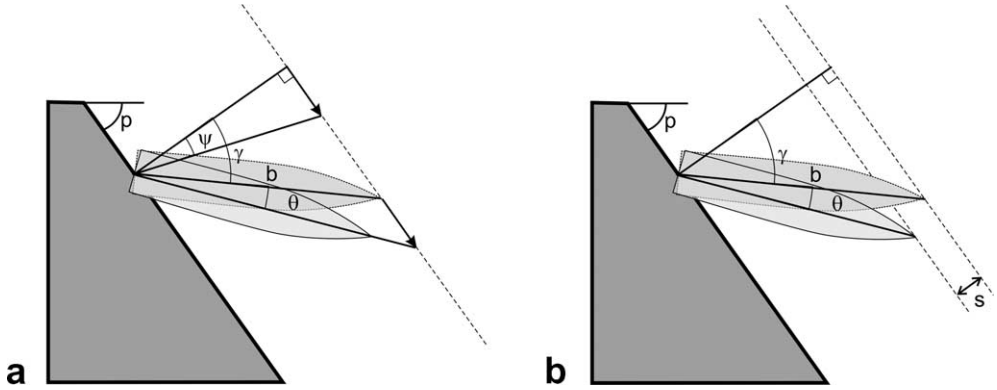

Fig. 6. Comparison between the tilt angles of a near-fault belemnite, in two endmember situations: (a) normal simple shear induced by drag folding along the fault, and (b) dissolution in the hanging wall along the fault. Vertical cross-section perpendicular to fault strike, belemnite in section plane. Belemnite in medium grey (initial position) or light grey (final position). Same parameters in (a) and (b): p, dip angle of fault, b, length of belemnite, γ, angle between belemnite axis and normal to fault plane, θ, tilt angle of belemnite. In the normal simple shear case (a), ψ is the shear angle. In the pressure-solution case (b), s is the equivalent thickness of dissolved rock along the fault.

of oblique geometry can be derived through additional consideration of the angle between belemnite trend and fault strike. Before deformation, the belemnite makes an angle γ with the normal to fault plane (Fig. 6). The sign of γ is determined according to the position of the belemnite in the quadrants bounded by the fault and the normal to fault (γ is positive in the situation of Fig. 6). Thus, the initial plunge of the belemnite is $\gamma+p-\pi/2$ (p being the fault dip, angles in radians). After deformation, the belemnite has rotated by an angle θ (with the same sign convention as before), so that it makes an angle $\gamma+\theta$ with the normal to fault plane (Fig. 6). Thus, the final plunge of the belemnite is $\gamma+\theta+p-\pi/2$.

4.3. Two-dimensional analysis: simple shear

In the shear case, the geometrical configuration (Fig. 6a) implies that the rotation angle of the belemnite, θ, is given by:

$$\tan\theta = \frac{\tan\psi\cos^2\gamma}{1+\tan\psi\sin\gamma\cos\gamma}. \quad (4)$$

For infinite simple shear ($\psi=\pi/2$), θ becomes close to $\pi/2-\gamma$, the largest possible rotation resulting in a belemnite parallel to fault plane. $\theta=\psi$ for a belemnite perpendicular to fault plane and $\theta=0$ for a belemnite parallel to fault plane. The usual width of the drag fold zone falls in the range 0.1–1 m, and the usual vertical offset ranges from 0.05 to 1 m (Fig. 4). The ratio between the fault-parallel displacement and the width of the drag fold zone usually ranges between 0.7 and 1.4, indicating shear angles (ψ) from 35 to 55°. Our data from non-faulted areas revealed that most belemnite plunges fall in the range 0–20°. Considering the usual fault dips (p) in these cross-sections, 70–80°, this range involves values from −10 to 40° for the angle γ defined above. With these bounds for ψ and γ, Eq. (4) implies that the rotation angle of the belemnites, θ, may vary from 17 to 61°.

How the belemnite orientation may vary after drag folding along the normal fault, as a function of the initial belemnite attitude, is illustrated in Fig. 7, based on a simple example with a 75° dipping fault and a rather large shear angle of 45°. The fossil rotation induced by simple shear is first shown for a belemnite with a pre-faulting plunge of 20° in the same direction as fault dip (Fig. 7a). The rotation calculated from Eq. (4) is 25°, resulting in a final plunge of 45°. For a belemnite with a pre-faulting plunge of 20° in the direction opposite to fault dip (Fig. 7b), the calculated rotation is 47°, resulting in a final plunge of 27°. It follows that in this particular situation (initial belemnite plunge up to 20°, $p=75°$, $\psi=45°$) the final angle between the belemnite and the dip line of the fault cannot be smaller than 30° (first case) or 48° (second case). However, our measurements in the studied area revealed a high proportion of belemnites being parallel to, or making small angles with, the dip lines of the normal faults. Such attitudes cannot be explained by drag folding along normal faults taken alone, which implies that the pressure-solution phenomena played a significant role.

The relationships between initial and final plunges of belemnites in the drag-fold zone along a normal fault are numerically displayed in Table 1 (left half), considering realistic values for fault dip (p: 60, 70, 80°), initial belemnite plunge (i_0: −30, −20, −10, 0, 10, 20, 30°) and shear angle

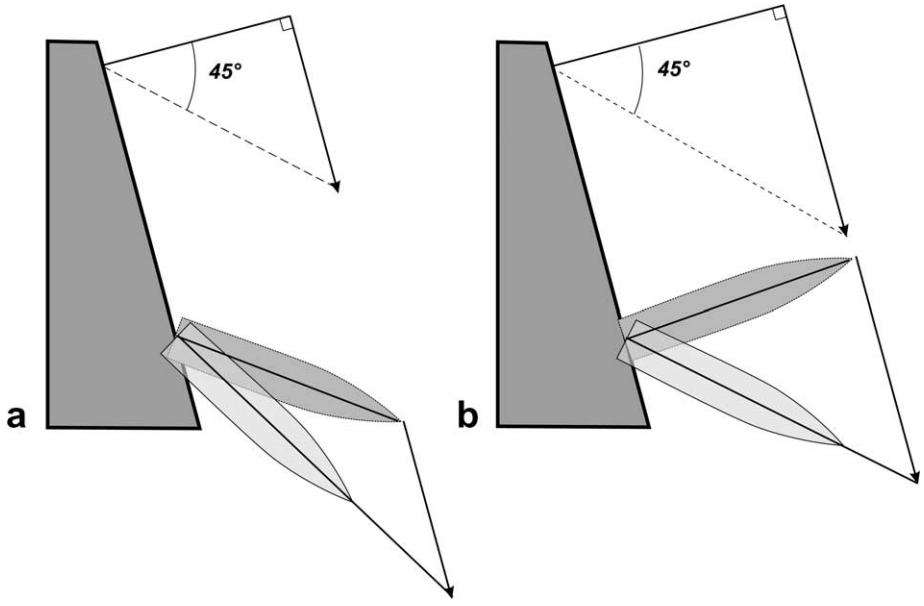

Fig. 7. Variations in belemnite tilt angle as a function of the initial belemnite plunge, in the case of drag folding along a normal fault. Simple shear is assumed within the fault-parallel zone that contains the belemnite. Two contrasting typical situations are shown. In both schemes the belemnite trends perpendicular to fault strike, the dip angle of the fault is 75° and the simple shear angle is 45°. The initial and final positions of the belemnite are shown in medium grey and light grey, respectively. The pre-faulting plunge of the belemnite is 20° in the same direction as fault dip in (a), and 20° in the direction opposite to fault dip in (b). With the same shear angle (as shown by upper triangles) the rotation is 25° in (a) and 45° in (b), giving final plunges of 45° and 25°, respectively. See also text.

Table 1
Determination of belemnite plunges after drag folding (light grey) or dissolution (medium grey) along a normal fault

	p	60	70	80	*p*	60	70	80
i_0	ψ	*i*	*i*	*i*	*s/b*	*i*	*i*	*i*
−30	45	15	19	22	0.25	11, −71	−42	−56
	55	25	31	37	0.5	30, 90	−81	−74
	65	35	43	51	0.75	46, 84	84	−89
	75	45	54	60	1	60	70	80
−20	45	20	25	29	0.25	13	21, −61	−52
	55	28	35	41	0.5	31	40, −80	−71
	65	37	45	53	0.75	46	56, 84	−86
	75	46	55	64	1	60	70	80
−10	45	24	30	35	0.25	16	23	31, −51
	55	31	38	45	0.5	34	41	50, −70
	65	38	47	55	0.75	49	56	66, −86
	75	46	56	65	1	60	70	80
0	45	28	34	40	0.25	22	26	33
	55	33	41	48	0.5	39	44	51
	65	40	48	57	0.75	53	59	66
	75	47	56	66	1	60	70	80
10	45	31	38	44	0.25	29	32	36
	55	36	43	51	0.5	45	49	54
	65	41	50	58	0.75	59	63	69
	75	48	57	66	1	60	70	80
20	45	35	41	48	0.25	37	39	42
	55	39	46	53	0.5	52	55	9
	65	43	51	60	0.75	60	69	73
	75	49	58	67	1	60	70	80
30	45	40	45	51	0.25	46	47	49
	55	42	49	56	0.5	60	62	65
	65	46	53	61	0.75	60	70	79
	75	50	59	68	1	60	70	80

Same configuration as in Fig. 2a and b, with belemnite trend perpendicular to fault strike. All angles in degrees. *p*, fault dip (as in Fig. 2). i_0, initial plunge of belemnite (positive towards hanging wall, negative towards footwall). *i*, final plunge of belemnite (same convention). Drag folding case: ψ, shear angle (as in Fig. 6a), rotation determined according to expression (4) in text. Pressure-solution case: *s/b*, ratio between removed thickness and belemnite length (as in Fig. 6b), rotation determined according to expression (5) in text; for belemnite perpendicular to fault surface, two final values given depending on sense of rotation.

(ψ: 45, 55, 65, 75°). Rather than average values, the tested shear angles have been selected along the most typical normal faults of the Mons Basin, according to the relationships between drag fold width and fault offset (e.g. 0.25–1 m for an offset of 1 m). The relationships of Table 1 are given in the two-dimensional case of a belemnite that trends perpendicular to fault strike (see the three-dimensional case at the end of this section).

4.4. Two-dimensional analysis: pressure-solution

We now consider the other end member of Fig. 2, the dissolution case. The rotation of the belemnite is calculated according to the scheme of Fig. 6b, giving:

$$\cos(\theta+\gamma)=\cos\gamma-\frac{s}{b}, \tag{5}$$

where b is the length of the belemnite while s, as defined before, is the corresponding thickness of rock that disappeared along the fault because of dissolution (the actual width of the dissolution zone is larger than s). The angles θ and γ are defined as before, but if γ is negative, θ is also negative. The absolute value of the term on the right side of Eq. (5) cannot be larger than 1, which corresponds to a condition of maximum possible rotation. This largest possible rotation (in radians), $\pi/2-|\gamma|$, results in a belemnite parallel to the fault plane.

Depending on the location and width of the along-fault pressure-solution zone, two types of pressure-solution phenomena should be distinguished. The first type involves asymmetrical dissolution across the fault, so that a belemnite located in the dissolution zone at a nonzero distance from the fault cannot undergo rotation until one of its tips reaches the fault surface. As a result, one simply obtains a minimum value of the removed width. The second type involves relatively homogeneous dissolution inside a zone parallel to the fault, so that the belemnite undergoes continuous rotation as dissolution continues, provided that it is contained inside this pressure-solution zone. Previous petrophysical analyses (Gaviglio et al., 1997) showed that the pressure-solution process commonly affects a fault-parallel zone that is about 0.10–0.15 m thick at present (which implies a larger original width).

The right half of Table 1 displays numerical relationships between initial and final plunges of belemnites (i_0 and i, respectively) in the pressure-solution zone along a normal fault. The values of p and i_0 considered in this two-dimensional exploration are the same as before. The values of the s/b ratio (s, rock thickness removed by dissolution and b, belemnite length) have been chosen according to the configurations observed in the Mons Basin. As noted before, pressure-solution results in steeper plunges, especially towards the footwall.

4.5. Three-dimensional analysis

The above formulations (4) and (5) as well as the values of Table 1 are given in two dimensions. However, the three-dimensional expression of the problem should be considered (Fig. 8), because most measured belemnites do not trend perpendicular to fault strike (Fig. 9). The angles that characterise the present-day orientation of a belemnite, α (trend with respect to fault strike) and ζ (plunge) are shown in Fig. 8a. In the vertical plane perpendicular to fault strike, the apparent plunge of a belemnite, ξ, is calculated as a function of α and ζ:

$$\tan\xi=\frac{\tan\zeta}{\sin\alpha}. \tag{6}$$

A straightforward treatment of the three-dimensional problem consists of defining a 'virtual' belemnite in a fault-perpendicular vertical plane. The trend of this virtual belemnite is perpendicular to fault strike, its plunge is ξ and its length, b', is $b\sin\zeta/\sin\xi$. The rotation that affected this virtual belemnite is characterised by θ, as given in expressions (4) for drag folding and (5) for pressure-solution, so that the pre-deformation plunge is ξ–θ (Fig. 8b$_1$). If θ is known, one determines the initial trend (α_0, relative to fault strike) and plunge (ζ_0) of the actual belemnite. Applying the formula (6) to the pre-deformation stage, one obtains:

$$\tan(\xi-\theta)=\frac{\tan\zeta_0}{\sin\alpha_0}. \tag{7}$$

The ratio between the lengths of virtual and actual belemnites, b'/b, is the same in both the pre-deformation (Fig. 8b$_1$) and post-deformation (Fig. 8b$_2$) stages. One infers that:

$$\frac{\sin\zeta}{\sin\xi}=\frac{\sin\zeta_0}{\sin(\xi-\theta)}. \tag{8}$$

Provided that the rotation angle, θ, has been calculated according to expression (4) or (5), the expression (8) gives ζ_0, and then expression (7) gives α_0. This systematic use of projection on fault-perpendicular vertical plane allows reconstruction of the pre-deformation stage. For exploration purposes, the same reasoning provides the post-deformation stage as a function of the initial configuration. One determines ξ_0 as a function of α_0 and ζ_0 according to formula (6), and then uses ξ_θ instead of $\xi_\theta-\theta$ and $\xi_\theta+\theta$ instead of ξ in expressions (7) and (8).

A complete three-dimensional solution has been written without using these shortcuts, but expressions are long because the rotation axes differ in the two processes considered. In the drag folding case, the rotation axis is the drag fold axis (along strike for a dip-slip fault) regardless of belemnite orientation. In the pressure-solution case, this axis is parallel to fault plane and perpendicular to belemnite, and hence depends on belemnite orientation.

The sensitivity of α to belemnite rotations is limited with respect to that of ξ, and the initial attitudes of the belemnites

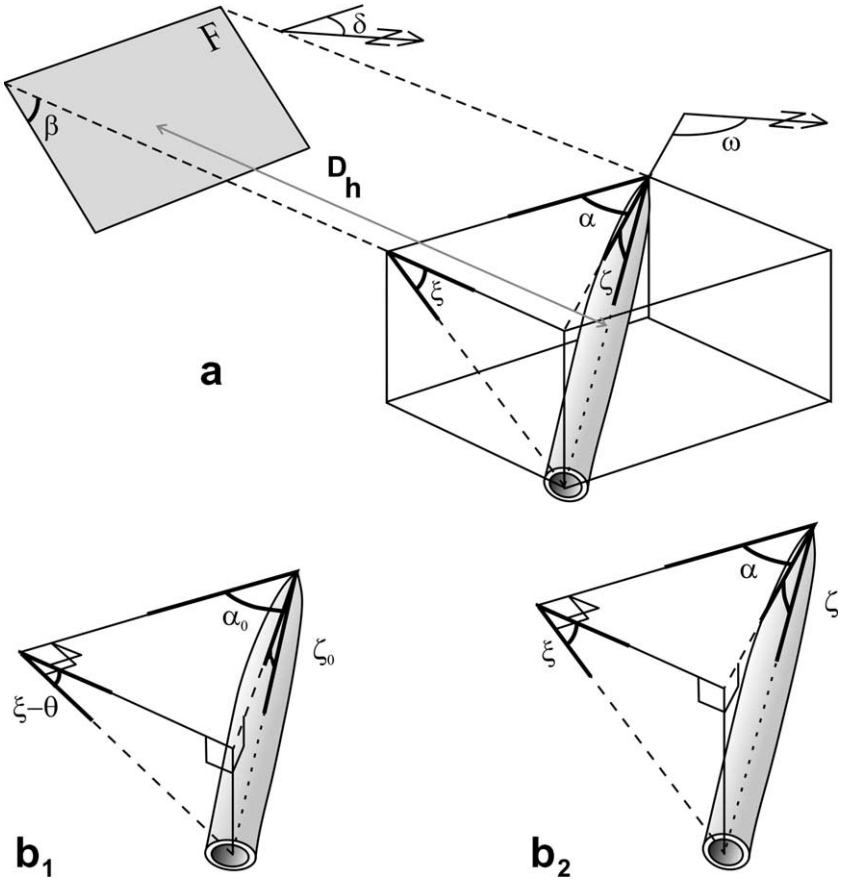

Fig. 8. Belemnite orientation with respect to fault. (a) Measured angles and symbols used. Trend and plunge of each measured belemnite as ω and ζ, respectively. Strike and dip of the closest fault plane (F, in grey) as δ and β, respectively. Distance from belemnite to fault is D_h. Comparing ω and δ, one obtains α (angle between belemnite trend and fault strike). Projection of belemnite on the vertical fault-perpendicular plane gives the apparent belemnite dip in this plane, ξ. (b) Three-dimensional solution of the problem, before (b_1) and after (b_2) rotation of belemnite by an angle θ. The angle $\xi-\theta$ thus becomes ξ, while the angles α_0 (initial belemnite trend relative to fault) and ζ_0 (initial belemnite plunge) are changed into α and ζ, respectively. The rotation angle (θ) and rotation axis depend on the deformation mode, drag folding or pressure-solution according to expressions (4) and (5), respectively.

are unknown (within dispersion bounds), so that the three-dimensional exploration of the problem is of little help in practice. In any case, the real spatial distribution of belemnites with respect to faults must be analysed to determine whether the distributions of belemnite plunges permits distinction between the two processes of Fig. 6.

5. Present-day distribution of belemnites

Our data collection in the white chalk in several open quarries of Harmignies and Obourg (Fig. 1b) included measurement of two angles for each belemnite: its trend, ω, and plunge, ζ. Our data (Fig. 8a) were collected along continuous sections, up to 100 m long, showing several normal faults. We measured, for each subset of belemnite data, the attitude of the closest fault or fracture, in terms of strike, δ, and dip, β. We subsequently determined for each belemnite the angle, α, between its trend and the fault strike. Consideration of this angle α, instead of azimuths δ and ω, allows direct comparison subsets of belemnites that correspond to faults with different trends. We also measured the horizontal distance, D_h, to the closest fault. The accuracy was about 0.01 m for distances smaller than 0.2 m, but larger uncertainties affected distance measurements taken at more than 0.2 m from the fault.

In addition, the pitch angles of the slickenside lineations on the normal faults were measured, showing that most faults are nearly dip-slip in type. The analysis of fault slip data is not shown in the present paper. Their geometry and mechanical significance have been described in previous papers (e.g. Vandycke and Bergerat, 1989), and highlight the trends of extension during and after the latest Cretaceous.

The stereoplot of Fig. 9a shows the distribution of 132 belemnite orientations in the white chalk at Harmignies and Obourg. This stereoplot shows first that there is no preferential trend of the belemnites in the horizontal chalk formation, and second that a majority of belemnites have shallow plunges. 77% of these plunges are shallower than 30°, including 60% shallower than 20°. This angular distribution is consistent with previous observations

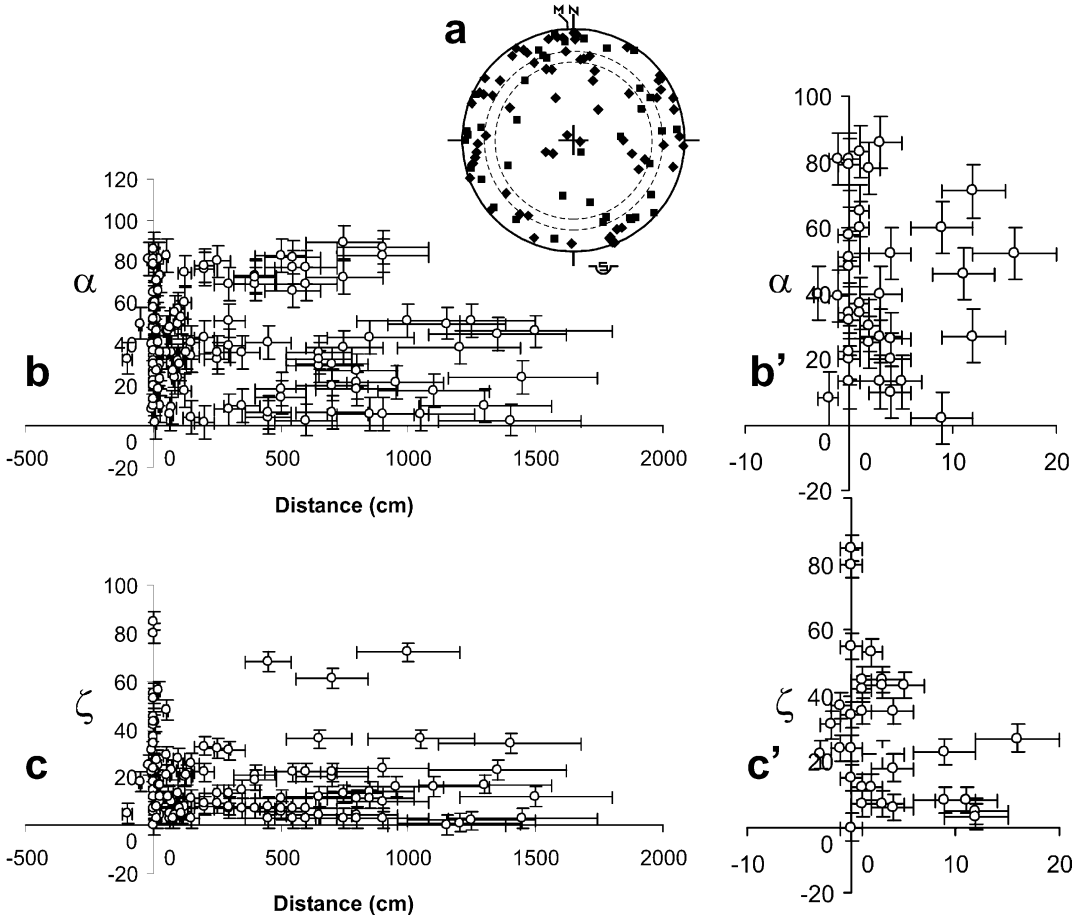

Fig. 9. Orientations of belemnites and their relationships with distance to fault in the 'Craie Blanche' (white chalk) of Harmignies–Obourg quarries. (a) Attitudes of measured belemnites in stereoplot, Schmidt's projection, lower hemisphere. Black squares for upward-pointing belemnites, black diamonds for downward-pointing ones. Dashed circles indicate 20 and 30° dips. (b) Distribution of angles α (degrees; belemnite trends with respect to fault strike, Fig. 8a) as functions of distance to fault, D_h (cm); error bars added. (b′) Magnified version of (b) for distances D_h shorter than 0.2 m. (c) Distribution of belemnite plunges, ζ (degrees), as functions of D_h (cm). (c′) Magnified version of (c) for D_h shorter than 0.2 m.

indicating that belemnites dying in the water or rejected by predators (Hauff, 1985) were falling without preferential orientation on the flat bottom of the chalk sea. A similar observation was made in undeformed lower Lias sediments near Charmouth, Dorset, southern England (Beach, 1979). Because our plunge data refer to all measured belemnites, including those affected by drag folding and pressure-solution strain along faults, the average plunge is steeper than that observed in non-faulted tabular areas of the Mons Basin, where plunges steeper than 20° are few, as noted in Section 4.

For the same data from Harmignies–Obourg, Fig. 9b shows the distribution of the values of α, the acute angle between fault strike and belemnite trend (as defined in Fig. 8a), as a function of the distance to the fault, D_h. Using α allows direct comparison between data subsets regardless of differences in fault strike. By convention, the distance D_h is noted positive in hanging walls and negative in footwalls (in Harmignies and Obourg, however, all distances larger than 1–5 m were noted positive because of ambiguities related to intersections of faults with different strikes). The number of data decreases as the distance to the fault increases, which principally reflects our interest for the attitudes of belemnites near the fault. Because of this observational bias, the variable density of belemnites is not significant in terms of spatial frequency of fossils at distances larger than a few metres from the faults. We, however, observed a high concentration of belemnites along and near the faults. The variation of belemnite density within 2 m from the faults is discussed in Section 6. The diagram of Fig. 9b indicates that there is no definite relationship between the angle α and the distance D_h to the fault. However, small angles are more numerous within distances smaller than 0.2 m from the fault (Fig. 9b and b′), which may reveal fault-related tilting resulting from drag folding or dissolution: both these processes tend to re-orient belemnites parallel to fault strike.

The distribution of belemnite plunges, ζ, as a function of the distance to the fault shows that plunges steeper than 20–30° are scarce at large distances from faults, but become common when the distance to fault is less than about 0.2 m (Fig. 9c and c′). Because the diagrams of Fig. 9b and c refer

to distances D_h in the range 0–15 m, magnified diagrams are shown to show details for distances smaller than 0.2 m (Fig. 9b′ and c′). They highlight the concentration of low values of α (especially 0–40° at distances less than 0.05 m) and high values of ζ (larger than 30° at distances less than 0.05 m) in the hanging wall close to the fault, which are both consistent with significant drag folding. However, as pointed out in Section 4, the presence of very large angles ζ (up to nearly 90°) along the fault cannot be explained by drag folding only and implies that dissolution has occurred.

To analyse in more detail the effect of drag folding and dissolution along normal faults, we collected two sets of data in the phosphatic chalk in the underground La Malogne quarries. The faults are well exposed so that uncertainties in distance measurements are small with respect to those from Harmignies–Obourg (Figs. 10 and 11; compare with Fig. 9). Large values of ζ are not common on the footwall, consistent with the poor development of drag folding there and suggesting little dissolution on this upthrown side. Most of our observations were consequently done on the downthrown side (hanging wall) of the normal faults.

The first set was collected from a site where numerous fossils could be observed at distances up to about 10 m from a single fault, the Ali Baba fault (Fig. 10). The distribution of 138 belemnite attitudes (Fig. 10a) resembles that observed at Harmignies–Obourg (Fig. 9a), with a majority of shallow plunges (64% of plunges shallower than 30°, including 57% of plunges shallower than 20°). Across the Ali Baba fault, we analysed in detail the distribution of belemnites as a function of the distance to fault, D_h, in terms of both the trends with respect to the fault (angle α; Fig. 10b) and the plunges (angle ζ; Fig. 10c). This distribution indicates that at distances larger than about 0.20 m in the hanging wall, the belemnite trends are randomly distributed, with shallow plunges (in the range 0–30°) and no preferential plunge towards or away from the fault. Both the Harmignies–Obourg and Ali Baba data sets thus highlight the distribution of belemnite attitudes in the absence of deformation, with random trends (Figs. 9b and 10b) and shallow plunges (Figs. 9c and 10c). Keeping this distribution of sedimentary origin in mind, we now focus on the near-fault distribution, in fault fringes where belemnites are affected by drag folding and dissolution, mainly in the hanging wall.

The second set is referred to as Bavay and includes scattered observations at short distances from 15 different faults (Fig. 11). The belemnite trends as function of the distance to fault (Fig. 11b) have been corrected, to allow comparison with reference to a unique fault strike. The distribution of belemnite attitudes shows dominant trends rather perpendicular to fault strikes, and a variety of plunges (Fig. 11a). The trend distribution results from both the observational bias with most data being collected along a cross-section perpendicular to fault strike and the predominance of data collected in the hanging wall at a distance less than 0.25 m from each fault. A majority of data thus reflects the distribution in the hanging wall fault fringe

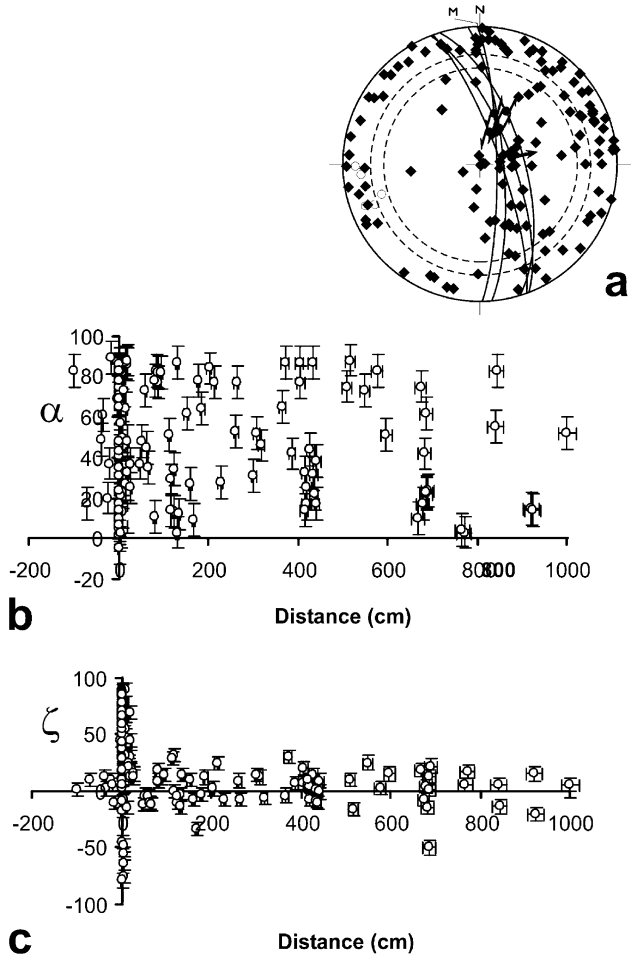

Fig. 10. Orientations of belemnites and their relationships with distance to a single fault, the Ali Baba Fault, in the phosphatic chalk of La Malogne quarry. (a) Attitudes of measured belemnites shown as black diamonds in stereoplot, Schmidt's projection of lower hemisphere. Dashed circles indicate 20 and 30° dips. Five typical measurements of the fault surface are shown as thin lines (fault) with dots and arrows (normal slickenside lineations). (b) Distribution of angles α (degrees), the belemnite trends with respect to fault strike, as functions of the distance to fault, D_h (cm), with error bars. (c) Distribution of belemnite plunges, ζ (degrees), as functions of D_h (cm). Note that the sign of ζ depends on the plunge towards or away from fault (negative and positive, respectively).

where drag folding and dissolution are predominant. In the hanging wall fringe, the belemnites show steep plunges, up to nearly 90° (Fig. 11c).

In Ali Baba (Fig. 10) and Bavay (Fig. 11), the belemnites sampled in the fault and at a close distance from it reveal a majority of plunge directions toward the hanging wall positive values of ζ). Most of the few fossils measured in the footwall also plunge toward the hanging wall (Figs. 10c and 11c). Along the faults, as already observed in the white chalk of Harmignies–Obourg, the Ali Baba and Bavay sites show a large proportion of steep hanging wall-verging plunges ζ (up to nearly 90°). Keeping in mind the limited plunge dispersion where faults are absent, this situation cannot be explained by drag folding taken alone, because of the relatively low amounts of simple shear constrained by

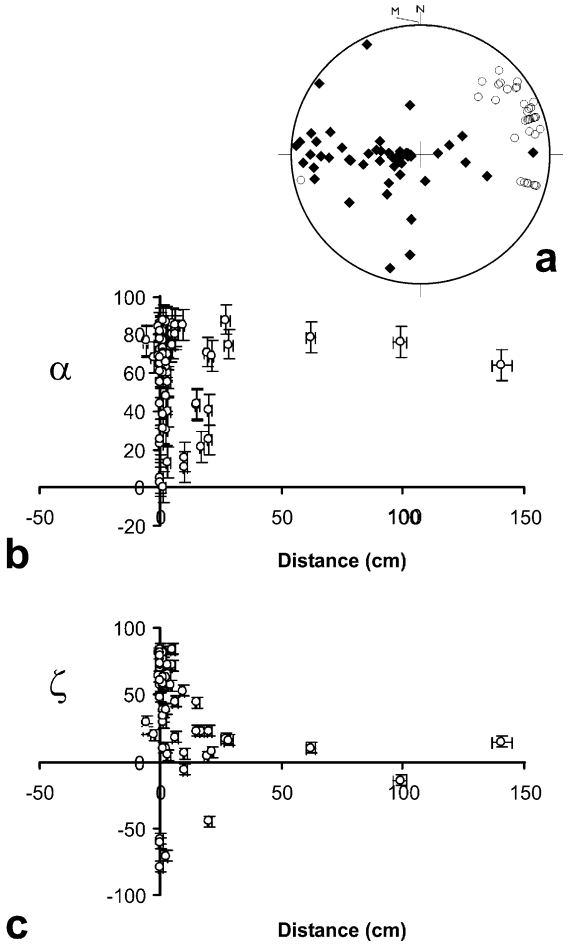

Fig. 11. Orientations of belemnites and their relationships with distance to several faults of the Bavay area, in the phosphatic chalk of La Malogne quarry. (a) Attitudes of measured belemnites shown as black diamonds in stereoplot, Schmidt's projection of lower hemisphere (open dots are poles to faults). (b) and (c) α and ζ as functions of D_h, same captions as for Fig. 10b and c, respectively.

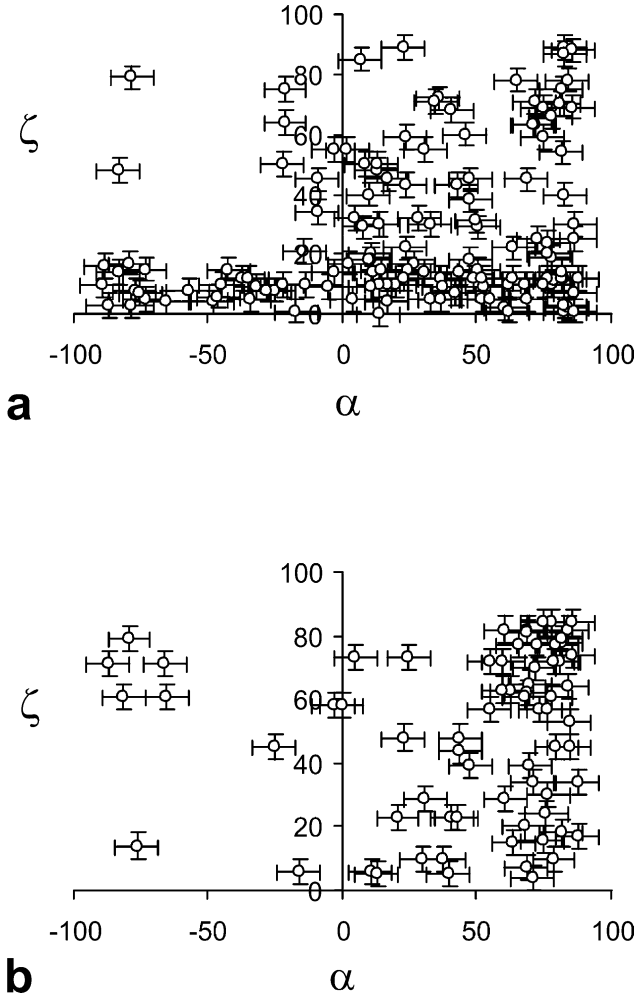

Fig. 12. Distribution of belemnite plunges, ζ (ordinates) as function of angles α (belemnite trends with respect to fault strike, abscissas) in the phosphatic chalk of La Malogne quarry. (a) Ali Baba Fault. (b) Faults of the Bavay area. All angles in degrees, error bars added. The sign of α depends on the plunge towards (−) or away from (+) fault.

the deformation zone width and offset. Had simple shear been fully responsible for the tectonic tilting of the belemnites, shallower plunges would have been observed near the fault (taking into account the depositional plunges of these fossils). Significant dissolution is indispensable to explain the large number of steep plunges observed near the faults, mainly in the hanging wall.

These orientation properties are summarised in Fig. 12, where the plunges of the belemnites (ζ, from 0 to 90°) are plotted against their trends relative to fault strike (α, from −90 to 90°). In this case α is noted as positive for hanging wall-directed plunges and negative for footwall-directed ones. The diagram from Ali Baba (Fig. 12a), where many measurements could be done at relatively large distances from the fault, shows that considering the plunge range 0–20°, there is a rather uniform dispersion of plunges for all directions. This is not the case in Bavay (Fig. 12b), because data were principally collected in the hanging wall fault fringes at very short distances from the fault. In both cases, steep plunges (from 30 to 90°) are mainly restricted to the right half of the diagram, indicating that they are hanging wall-verging. The steepest plunges (60–90°) correspond to large positive angles α (60–90°), consistent with maximum hanging wall-verging tilt affecting near-fault belemnites that trend at large angles to fault strike. This conclusion is valid in Ali Baba, where numerous galleries allowed spatially significant collection of belemnite trends; it is not in Bavay, where an observational bias affected the trend measurements along a planar cross-section perpendicular to fault strike (Fig. 11a). Despite the 20–30° sedimentary dispersion in plunges and the measurement uncertainties, the correlation between α and ζ distributions shown in Fig. 12 indicates that the fault-related deformation, including dissolution effects, is responsible for most large tilts of the belemnites.

To further investigate this distribution, it is appropriate to examine for each belemnite the component of plunge

in the direction perpendicular to fault strike. Because the normal faults studied are dip-slip, this component is an expression of the drag folding and/or dissolution effects. We thus use the apparent belemnite plunge, ξ, in a vertical plane perpendicular to fault strike (Fig. 8a), as defined in expression (6). This expression implies that ξ cannot be calculated for belemnites that trend parallel to fault strike or vertical belemnites, a minor restriction considering the data. More important is the bias introduced by the direction of the belemnite relative to the fault: a value of ξ close to 90° can be obtained with a shallow belemnite plunge, provided that the belemnite trends parallel to, or at a small angle with, the fault strike. Such an apparent plunge of 90° has no significance in terms of tilt. This restriction explains why large values of ξ may persist at large distances from the fault. To limit this bias, all data that correspond to angles α smaller than 45° have been removed in Fig. 13. The remaining data (i.e. belemnites that trend oblique at large angles to the fault) show that angles ξ reach large values, up to 90°, along the faults, whereas at large distances ξ remains smaller than 30°. It has been previously pointed out, qualitatively (Section 4, Fig. 5) and quantitatively (this section, Figs. 9–11), that along the faults the belemnite plunges are too steep to be accounted for by normal simple shear related to drag folding. The same observation is made at all sites with the angles ξ (Fig. 13). It implies that pressure-solution phenomena have also been involved along these faults.

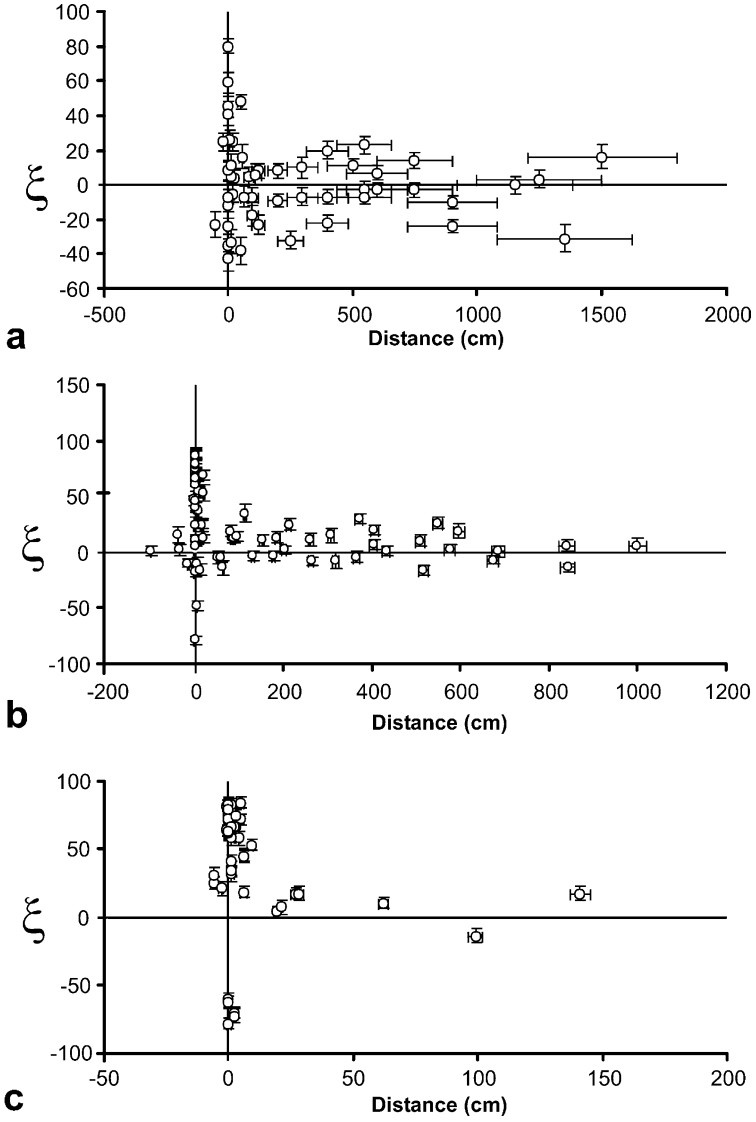

Fig. 13. Distribution of belemnite apparent plunges in cross-sections perpendicular to fault strikes, ξ (ordinates), as function of distance to fault (D_h in Fig. 8a). Data from belemnites with angles α smaller than 45° have been removed. (a) Harmignies–Obourg quarries. (b) Ali Baba Fault. (c) Faults of the Bavay area. Angles in degrees, error bars added.

6. Discussion

In two major sub-areas of the Mons Basin, the analysis of belemnite orientations in the white chalk (Harmignies–Obourg) and the phosphatic chalk (Ali Baba–Bavay) has shown high correlation between steep belemnite attitudes and normal faults. The initial distribution of belemnite attitudes after sedimentation is reconstituted in non-deformed layers far from faults, showing that except for a few fossils, their depositional plunges remain shallower than 20–30° (Figs. 9 and 10). Steeper plunges, up to 90°, are correlated with fault occurrence, indicating that belemnites have been tilted as a result of normal faulting, mainly in the hanging wall at distances smaller than about 0.2 m from the fault (Figs. 9–11). At the Ali Baba site, the only exception among the 138 measured fossils is a belemnite with a 50° plunge at a distance of 7 m from the fault (Fig. 10c). In the white chalk of Harmignies–Obourg, the distribution is similar but exceptions occur, with few plunges steeper than 30° at distances larger than 0.2 m from the faults (Fig. 9c). These exceptions should not be regarded as significant because in these quarries dissolution may have occurred along joints (in addition to faults) and be responsible for these local steep plunges. Most steep plunges are observed along the faults themselves (Fig. 9c′). Although data at distances larger than 0.3 m are few at Bavay, the distribution of plunges as a function of the distance resembles those of Ali Baba and Harmignies–Obourg (Fig. 11c).

Fig. 12 shows a correlation between values of α (the angle between fault strike and belemnite trend) close to 90° and the steepest belemnite plunges (ζ) at the Ali Baba and Bavay sites. The strongest tilts, up to 90°, affected belemnites that trended at large angles with respect to fault strike. This correlation brings further confirmation of the tectonic origin of tilt, for plunges larger than 20–30° (Fig. 12). Besides, most belemnites trending at large angles to fault strike plunge towards the hanging wall, consistent with fault drag and dissolution effects. These geometrical characteristics are highlighted in Fig. 13, showing the apparent tilt of belemnites, ξ, as a function of distance in a fault-perpendicular cross-section.

No significant influence of the fault-related tilt process was detected at distances larger than 0.2–0.3 m from fault. For this reason we focussed on the near-fault distribution of belemnites attitudes. Fig. 14 shows this distribution of angles ξ (as defined in Fig. 8a) at all observation sites, for all belemnites that trend at an angle larger than 45° with respect to fault strike. Because the normal faults are dip-slip in type, this diagram enables one to reasonably evaluate the amounts of fault-related tilt, despite the bias introduced by the up to 20–30° initial plunges of belemnites that resulted from deposition processes. The largest angles ξ, in the range 60–90°, are found in the hanging wall at distances smaller than 0.05 m from the fault. At distances from 0.05 to 0.2 m, the largest angles ξ reach 55° (with one exception at 70°). As pointed out earlier, at distances larger than 0.2 m, most angles are smaller than 20–30° (Fig. 13), which simply reflects the absence of fault-related tilting.

At a close distance to the fault in the hanging wall a minor but significant number of belemnites steeply plunge towards the fault. This is illustrated in Fig. 14 by the negative values of ξ for distances smaller than 0.1 m. Had drag folding and normal simple shear been the sole source of tilting, these steep plunges towards the fault would be impossible to explain considering both the shallow pre-faulting plunges of the belemnites and the influence of

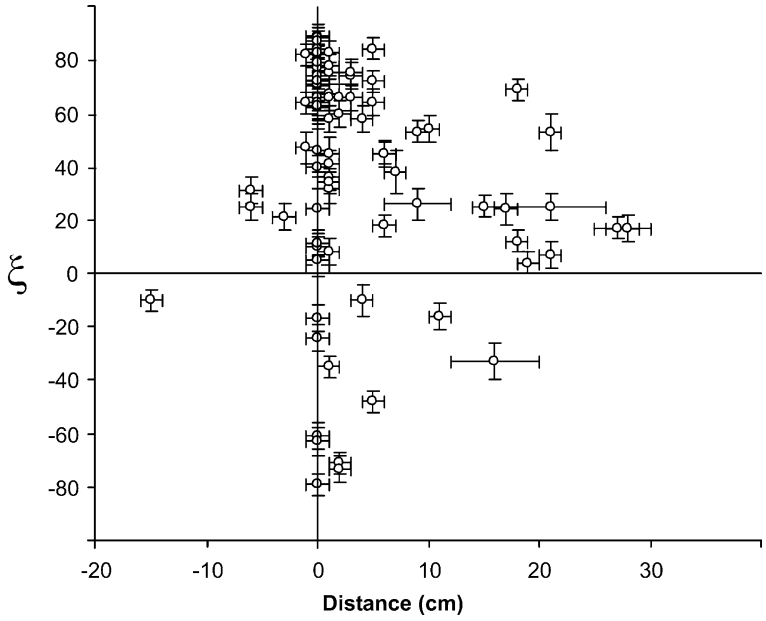

Fig. 14. Relationships between apparent plunges of belemnite in cross-sections perpendicular to fault strikes, ξ (ordinates), and distances to fault (D_h in Fig. 8a), for distances less than 0.2 m (footwall) and 0.3 m (hanging wall). Same data as for Fig. 13, all sites together. Angles in degrees, error bars added.

simple shear on plunge changes as discussed in Section 4 (Fig. 6). On the contrary, the pressure-solution well accounts for such steep plunges. This contrast is shown in Fig. 15 with a normal fault that dips 80° (a usual fault dip in the studied area) and a belemnite that initially plunged 20° towards the fault (giving $\gamma = -10°$). Fig. 15a shows the drag folding case with a shear angle $\psi = 30°$: expression (4) yields a rotation (θ) of 32° clockwise, giving a final plunge of 12° away from the fault. Fig. 15b shows the pressure-solution case with a dissolved width (s) four times smaller than the belemnite length (b): expression (5) yields an anticlockwise rotation of 43°, giving a final plunge of 53° towards the fault. This simple example highlights the potential of dissolution process to generate steep belemnite plunge towards the footwall, a situation that drag folding fails to account for.

Comparing the two sides of a fault, Fig. 14 shows that for belemnites that plunge towards the fault angles ξ steeper than 50° (up to 80°) are found within a 0.05-m-wide hanging wall fault fringe. For belemnites that plunge away from the fault the same values are found within a distance slightly larger than 0.2 m in the hanging wall. Because dissolution is the only process related to faulting that can produce steep footwall-verging belemnite plunges in the hanging wall, this distribution suggests that the present-day width of the fault fringe affected by dissolution is about 0.05 m. For belemnites that plunge away from the fault, angles ξ steeper than 65° (up to 90°) are found within a 0.05-m-wide hanging wall fault fringe, which also reveals dissolution, in agreement with the discussion of steep plunges in Section 4.

The width of the zone affected by drag folding is about 0.2 m, and the plunge values attributed to simple shear (according to their distance to fault larger than 0.05 m) are small in comparison with the values discussed above (angles ξ up to 65° at distances from 0.05 to 0.2 m; see Fig. 14). For instance, taking a dip of normal fault, 75°, a depositional belemnite plunge of 20° towards the hanging wall (giving $\gamma = 35°$) and a simple shear angle of 55°, one obtains with simple shear a rotation angle $\theta = 30°$ (Eq. (4)), giving a final belemnite plunge of 50° towards the hanging wall. In the distance range 0.05–0.2 m, this theoretical value well fits the average observed value for ξ angles that are too large to be attributed to depositional plunge dispersion (Fig. 14). According to this evaluation drag folding is unlikely to produce tilt angles from 65 to 90° in the studied sections of the Mons Basin.

It has been shown above that drag folding along normal faults cannot explain the steep belemnite plunges commonly observed in the normal fault zones of the Mons Basin. We infer that the along-fault dissolution has played a major role in the normal faulting that affected this basin during the Campanian, Maastrichtian and Danian times. Although further quantification of the proportion between pressure-solution and drag folding is difficult because of complex interaction and initial dispersion of belemnite plunges, consideration of present-day belemnite plunges brings strong constraints. As Fig. 14 shows, angles ξ up to 85–90° towards the hanging wall are common within distances of about 0.05 m from the fault (downthrown side), with many rostra trending perpendicular to fault strike. In the absence of drag folding, and assuming that the fossils were deposited horizontally, vertical belemnite attitudes imply that the width of dissolved material cannot be less than the length of belemnite remnants, about 0.05–0.06 m in most cases. Even a depositional plunge of 20 or 30° cannot vitiate this estimate by more than 6 or 13% (respectively). Drag folds exist, but the presence of angles ξ up to 80° towards the footwall as well as the hanging wall within the same distance of 0.05 m from the fault in the downthrownblock (Fig. 14) cannot be explained by drag folding. We infer that the most important source of large belemnite tilts is the pressure-solution process.

7. Conclusion

The large numbers of belemnites in the upper Cretaceous of the Mons Basin allowed us to quantify the orientation patterns of these fossils far away from, and close to dip-slip normal faults. The comparison between the depositional dispersion of belemnite orientations and their near-fault

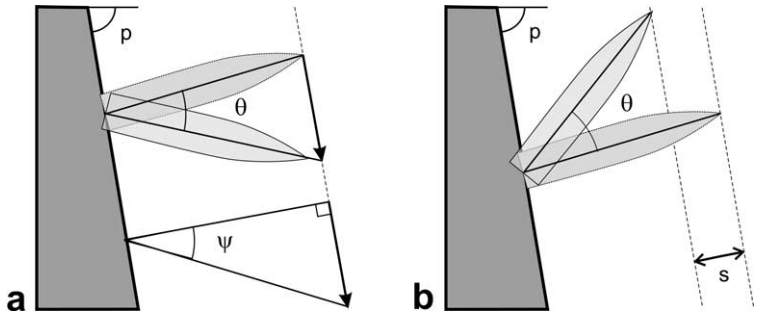

Fig. 15. Contrast between effects of drag folding associated with normal simple shear (a) and along-fault dissolution in hanging wall (b). Vertical cross-section perpendicular to fault strike. Belemnite in section plane in medium grey (initial position) or light grey (final position). p, dip angle of fault, ψ, shear angle of fault, s, equivalent thickness of dissolved rock, θ, tilt angle of belemnite. Note the opposite senses of belemnite rotation for (a) and (b).

distributions led us to identify the nature of deformation along the faults. This deformation results from two processes that occurred before complete lithification: drag folding and pressure-solution. Several cross-sections reveal drag folds along normal faults and allow quantification of simple shear. Although the existence of pressure-solution processes had been ascertained by petrophysical studies, quantification was difficult in the absence of clear structures (e.g. stylolites). We consequently examined the belemnites, which are much less affected by dissolution than the surrounding chalky matrix. A detailed analysis of the distribution of belemnite orientations as a function of distance to fault allowed us to evaluate the importance of each of the two processes involved. We explored the geometrical effects of drag folding and pressure-solution, and we applied the results to our data sets. Despite depositional dispersion in fossil trends and plunges, some features unambiguously reveal that pressure-solution played a major role. This is the case of steep belemnite plunges towards the footwall, which cannot be produced by drag folding. On the other hand, the frequency difference between angles towards hanging wall and footwall partly results from drag folding.

Quantifying these aspects was subject to many difficulties. The distribution of fossil density as a function of distance to fault could not be used as a reliable marker of dissolution, because the syndepositional character of many normal faults may have affected the dispersion of the fossils, with belemnite accumulating at the foot of small fault scarps during sedimentation. This syndepositional aspect might also bias the plunge distribution, with many belemnites plunging towards the downthrown side because of fault scarp slope.

Despite these difficulties, the analysis of belemnite orientation distribution revealed significant trends. Our results suggest a minimum dissolved thickness of 0.05 m across the observed normal faults. In the Mons Basin most normal faults have steep dips (75–80°), so that the transverse horizontal displacement represents 18–27% of the vertical offset. With the vertical offsets observed in the studied outcrops (0.1, −1 m), the transverse horizontal displacement falls in the range 0.02–0.27 m. This comparison indicates that the extension could well be compensated by the pressure-solution effect (Fig. 2b). In this respect, it is appropriate to mention that some authors put emphasis on the role of vertical movements in the Mons Basin (Delmer, 1972; Dupuis and Vandycke, 1989). Although the existence of extension in the West European platform during the latest Cretaceous is beyond doubt (e.g. Vandycke, 2002), our evaluation of the pressure-solution process across normal faults suggests that in the case of the Mons Basin the amount of extension inferred from normal fault geometry is probably overestimated. Our analysis also confirms that pressure-solution across faults may induce significant volume changes even in the absence of clear structural expression (e.g. stylolites), and thus deserves careful interest in deformation analyses.

Acknowledgements

This study was supported by the France–Belgium research project ‘Tournesol’. Help by Freddy Leclercq, leader of the La Malogne quarry group, who passed away in 2003, and work permission from CCC, CBR and Obourg quarries, are gratefully acknowledged. We also thank Dr Andrea Billi, Dr Jean-Pierre Gratier and the Editor, Dr Thomas Blenkinsop, for constructive comments.

References

Beach, A., 1979. The analysis of deformed belemnites. Journal of Structural Geology 1, 127–135.

Carrio-Schaffhauser, E., Gaviglio, P., 1990. Pressure-solution and cementation stimulated by faulting in limestones. Journal of Structural Geology 12, 987–994.

Clayton, C.R.I., Matthews, M.C., 1987. Deformation, diagenesis and the mechanical behaviour of chalk. In: Jones, M.E., Preston, R.M.F. (Eds.), Deformation of Sediments and Sedimentary Rocks. Geological Society Special Publication, 29, pp. 55–62.

Colbeaux, J.P., 1974. Mise en évidence d’une zone de cisaillement Nord-Artois. Comptes Rendus de l’Académie des Sciences de Paris 278, 1159–1161.

Delmer, A., 1972. Origine du bassin crétacique de la vallée de la Haine. Professional Paper. Geological Survey of Belgium 1972-5.

Dunne, W.M., Hancock, P.L., 1994. Palaeostress analysis of small-scale brittle structures. In: Hancock, P. (Ed.), Continental Deformation. Pergamon Press, Oxford, pp. 101–120.

Dupuis, C., Vandycke, S., 1989. Tectonique et karstification profonde: un modèle original pour le Bassin de Mons. Annales de la Société Géologique de Belgique 112, 479–487.

Gaviglio, P., Chayé D’Albissin, M., Bergerat, F., Vandycke, S., 1993. Failles et modification de texture dans la craie: un exemple de graben dans le bassin de Mons (Belgique). Bulletin de la Société Géologique de France 163, 565–575.

Gaviglio, P., Adler, P., Thovert, J-F., Vandycke, S., Bergerat, F., Bekri, S., Lestideau, R., 1997. Grain-scale microstructures and physical properties of faulted chalk. Bulletin de la Société Géologique de France 168, 727–739.

Gaviglio, P., Vandycke, S., Schroeder, C., Coulon, M., Bergerat, F., Dubois, C., Pointeau, I., 1999. Matrix strains along normal fault planes in the Campanian white chalk of Belgium: structural consequences. Tectonophysics 309, 41–56.

Gratier, J.P., 1987. Pressure-solution creep and associated tectonic differentiation in sedimentary rocks. In: Jones, M.E., Preston, R.M.F. (Eds.), Deformation of Sediments and Sedimentary Rocks. Geological Society Special Publication, 29, pp. 25–38.

Hancock, P.L., 1985. Brittle microtectonics: principle and practice. Journal of Structural of Geology 7, 437–457.

Hauff, R.B., 1985. Urweltmuseum Hauff Holzmaden. Sonderausstellung Weichteilbelemniten, Holzmaden, 14pp.

Marlière, R., 1970. Géologie du Bassin de Mons et du Hainaut. Un siècle d’histoire. Annales de la Société Géologique du Nord 90, 171–189.

Mimran, Y., 1977. Chalk deformation and large-scale migration of calcium carbonate. Sedimentology 24, 333–360.

Peacock, D.C.P., Fisher, Q.J., Willemse, E.J.M., Aydin, A., 1998. The relationships between faults and pressure-solution seams in carbonate

rocks and the implication for fluid flow. In: Jones, G., Fisher, Q.J., Knipe, R.J. (Eds.), Faulting, Fault Sealing and Fluid Flow in Hydrocarbon Reservoirs. Geological Society London, Special Publication, 147, pp. 105–115.

Ramsay, J.G., 1977. Pressure-solution—the field data. Journal Geological Society London 134, 72.

Robaszynski, F., Christensen, W.K., 1989. The Upper Campanian–Lower Maastrichtian chalks of the Mons Basin, Belgium: a preliminary study of belemnites and foraminifera in the Harmignies and Ciply areas. Geologie in Mijnbouw 62, 75–82.

Vandycke, S., 1992. Tectonique cassante et paléo-contraintes dans les formations crétacées du Nord-Ouest européen. Implications géodynamiques. Ph thesis, University of Paris VI.

Vandycke, S., 2002. Paleostress records in Cretaceous formations in NW Europe: synsedimentary strike-slip and extensional tectonic events. Relationships with Cretaceous–Tertiary inversion tectonics. Tectonophysics 357, 119–136.

Vandycke, S., Bergerat, F., 1989. Analyse microtectonique des déformations cassantes dans le Bassin de Mons. Reconstitution des paléochamps de contrainte au Crétacé-Tertiaire. Annales de la Société Géologique de Belgique 112, 479–487.

Vandycke, S., Bergerat, F., Dupuis, C., 1988. Paléo-contraintes à la limite Crétacé-Tertiaire dans le Bassin de Mons (Belgique). Implications cinématiques. Relations avec la Zone de Cisaillement Nord-Artois. Comptes Rendus de l'Académie des Sciences de Paris 307, 303–309.

Vandycke, S., Leclercq, F., Dupuis, C., Bergerat, F., Robaszynski, F., 1990. Tectonique et sédimentation à la limite Crétacé-Tertiaire dans le Bassin de Mons. Visite des carrières souterraines de la Malogne. Cadre stratigraphique et tectonique. Bulletin d'Information des Géologues du Bassin de Paris 27, 53–66.

Vandycke, S., Bergerat, F., Dupuis, C., 1991. Meso-Cenozoic faulting and inferred paleostresses of the Mons Basin (Belgium). Tectonophysics 192, 261–271.